# Image Charge Detection Mass Spectrometry: Pushing the Envelope with Sensitivity and Accuracy

John W. Smith, Elizabeth E. Siegel, Joshua T. Maze, and Martin F. Jarrold*

Chemistry Department, Indiana University, 800 E. Kirkwood Avenue, Bloomington, Indiana 47401, United States

ABSTRACT: A novel image charge detection mass spectrometer (CDMS) with improved sensitivity and mass accuracy is described. The improved detector design and method of data analysis allow us to measure a reliable mass for a single macroion that is an order of magnitude smaller than previously achieved with CDMS. The apparatus employs an image charge detector array consisting of 22 detectors. The detectors are divided into two groups that can be floated at different potentials. The signals from the detector array are analyzed using a correlation approach to yield the velocities in the two groups of detectors and the charge. These quantities, together with the voltage difference between the two groups of detectors, provide a value for the mass. The mass, m/z, and charge distributions recorded for 300 kDa poly(ethylene oxide) (PEG) are presented. The mass distribution shows a peak at around 300 kDa with a width close to that expected from the polymer size distribution. In addition, there are broad peaks in the mass distribution at around 100 and 500 MDa. The 300 kDa ions have m/z ratios of ~2 kDa/e, and the 100 and 500 MDa ions have m/z ratios of ~40 kDa/e. The 100 and 500 MDa ions probably result from PEG aggregates that are either present in solution or the residue of large electrospray droplets.

⟹ m/z and z for each ion
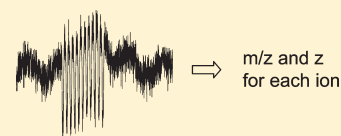
Two major challenges in mass spectrometry are measuring masses of large objects (i.e., masses in the 1 MDa to 1 GDa range) and determining mass distributions for mixtures such as polymers and nanoparticles. In the case of large objects, detector sensitivity and mass heterogeneity are the major stumbling blocks. Some progress has been made with nanomechanical mass sensors,[1,2] but it remains to be seen how competitive this technology will be. In the case of mixtures, it is the complex spectrum of overlapping peaks resulting from different masses and charge states that provides the road block. In principal, this problem could be overcome by very high resolution. Both of these challenges, however, can be addressed using charge detection mass spectrometry (CDMS).

Image charge detectors permit the simultaneous measurement of the charge and velocity of a macroion. If the energy is known, this can be used with the measured velocity to determine the m/z ratio. The m/z ratio can then be combined with the measured charge to yield a mass for each individual ion. This approach can be contrasted with conventional mass spectrometry where an m/z spectrum is recorded. Then, in order to determine the mass, the charge must be deduced from the m/z spectrum. For a macroion, this is accomplished by analyzing the series of peaks in the m/z spectrum resulting from different charge states. The separation between the peaks provides the charge. This approach is problematic for mixtures, as noted above.

In its most basic form, an image charge detector consists of a conducting tube connected to a charge sensitive preamplifier. As a charged object enters the cylinder, it impresses an image charge onto the cylinder which is detected by the preamplifier. If the cylinder is long enough, the image charge provides a measure of the charge on the object, and the time between when the object enters the cylinder and when it leaves provides a measure of the velocity. The problem with this elegantly simple approach is that it depends on directly measuring the charge on a single macroion.

The first use of an image charge detector to determine mass was in 1960 when it was used to determine the masses of microparticles for hypervelocity impact studies.[3-5] In this application, the microparticles were charged, accelerated, and passed through an image charge detector. The measured velocity and charge along with the known acceleration voltage provide the mass of each microparticle. Hendricks used a similar approach to measure the charges and masses of liquid droplets generated by electrospray in vacuum.[6] In the mid 1990s, Fuerstenau, Benner, and their collaborators used image charge detection to perform mass measurements on Megadalton molecular ions such as large DNA fragments and electrosprayed viruses.[7-9] In their implementation, the ions were generated by an electrospray source and accelerated by a voltage gradient before traveling through the image charge detector.

Electrical noise limits the accuracy of the charge measurements. Fuerstenau and Benner used a Gaussian differentiation peak shaping technique and reported a root mean square (rms) noise of 150 e. A more accurate value for the charge can be obtained by averaging over a series of measurements. This approach was implemented by Benner who used a linear trap to repetitively measure the charge of a trapped macroion.[10] The uncertainty in the charge measurement is expected to decrease as $n^{-1/2}$ where n is the number of measurements. Benner reported as the rms noise of 50 e which is reduced to 2.3 e for an ion that oscillates 450 times (the maximum number observed). However, for these experiments, the macroion must possess a charge of at least 250 e because the signal must be large enough to know when an ion passes through the image charge detector so that it can be trapped.
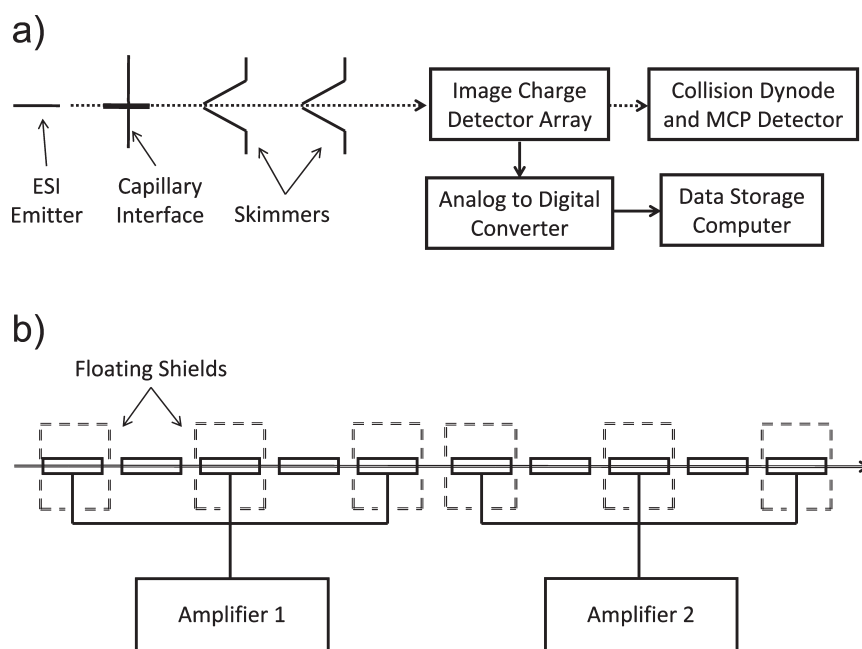
A

Figure 1. Schematic diagram showing (a) an overview of the experimental apparatus and (b) details of the electrical layout of the charge detector array.

Another way of performing multiple image charge measurements is to use a linear array of charge detectors. This approach was first realized by Gamero-Castaño.[11] He used a detector consisting of six collinear tubes with tubes 1, 3, and 5 connected to one amplifier (1) and tubes 2, 4, and 6 connected to another (2). The output from the amplifier 2 is subtracted from amplifier 1. With this arrangement, the detection limit in the time domain is $2^{1/2}$ lower than a single detector and the noise is $n^{1/2}$ lower (where n is the number of detectors). A noise level of around 100 e was reported for analysis in both the time and frequency domains for typical signals.

In this manuscript, we describe an image charge detector array consisting of 22 charge detection tubes. These tubes are arranged coaxially and divided into two sets of 11 detectors. The two sets of detectors are electrically isolated, and they are operated at different potentials. Measurement of the velocities in the two sets of detectors provides a measure of m/z without knowledge of the initial ion energy. This simplifies the ion source and eliminates the need for a monoenergetic ion beam. Ions undergo aerodynamic acceleration in the electrospray interface, leading to a distribution of initial velocities. While it is possible to accelerate the ions to minimize the effect of the initial velocity distribution, the accuracy of the charge measurement decreases as the ion velocity increases.

We use a correlation approach to analyze the output from the image charge detectors. This method offers significant advantages over a Fourier transform in terms of signal-to-noise ratio for the signals obtained here. Using correlation analysis, the rms noise level achieved with the 22 detectors is around 10 e for a 500 m/s ion. While the noise level is a factor of 4 worse than the best achieved by Benner with a recirculating trap, the linear array offers distinct advantages in terms of simplicity, throughput, and detection limit.

■ OVERVIEW OF THE EXPERIMENTAL APPARATUS

The experimental apparatus is shown schematically in Figure 1a. Ions are generated with an electrospray source and transferred into vacuum through a capillary interface. The electrospray needles were pulled from borosilicate glass capillaries. The electrospray voltage was applied to the solution through a stainless steel wire. A syringe pump provided a flow rate of 20 μL/h. The electrospray solution was 50:50 v/v water and methanol with 0.5% acetic acid and poly(ethylene oxide) (PEG; MW 300 000, Polysciences, Inc.) added to a concentration of 1.0 μM. The gas flow into the vacuum chamber is limited by a 15 cm long stainless steel capillary with an internal diameter of 0.75 mm. The copper block holding the capillary is heated to around 110 °C by cartridge heaters. Two conical skimmers are aligned coaxially with the capillary to provide two differentially pumped regions.

The expansion of the gas as it travels through the capillary causes an aerodynamic acceleration of the entrained ions. The aligned skimmers, combined with the 0.5 mm diameter aperture at the beginning of the detector array, only allows ions to enter the detector if they are within an acceptable angle to pass cleanly through the entire array. An ion detector, consisting of an orthogonal collision dynode and a pair of microchannel plates, is located after the charge detector to assist in optimizing the electrospray source. The source is adjusted to provide 10−100 ions/second at the ion detector. The ions enter the charge detector array at random intervals (i.e., they are not gated).

■ CHARGE DETECTOR ARRAY

The charge detector array consists of 22 image charge detector tubes separated by identical tubes set to the potential of the shielding. The detector tubes are divided into two groups as illustrated in Figure 1b. Each set is connected in parallel to a single amplifier, and the sets are electrically isolated from each other and from ground; a potential difference is applied between the sets. The ions travel at different velocities in the two sets of detectors, and the velocity difference, along with the potential difference, allows the m/z ratio to be determined without knowledge of the ions kinetic energy. With charge detection technology, the critical performance parameter to control is measurement
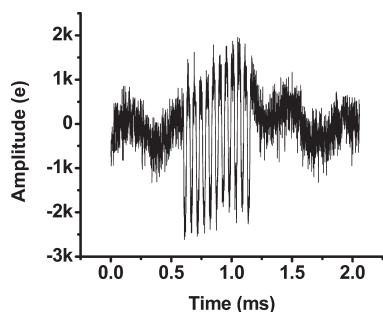
B

dx.doi.org/10.1021/ac102633p |*Anal. Chem.* XXXX, XXX, 000–000

Figure 2. Unprocessed signal for a macroion with a charge of around 2500 e traveling through the first group of detectors in the charge detection array.

time, which is set by the ion's velocity. In a heterogeneous mixture of ions with different masses and m/z values, different kinetic energies are required to achieve the same velocity. Therefore, instead of setting the kinetic energy, we allow the ion velocity to be set by the aerodynamic expansion at the capillary interface. For the results reported here, the second set of detectors is floated while the first is set to ground.

The individual tubes in the charge detector array were modeled in COMSOL Multiphysics (COMSOL, Inc.) and SIMION[12] to optimize their performance. The critical parameters in the design of a single unit for use in an array are as follows: capacitance to ground, signal rise time, electrical shielding, quantity of insulator material, and dead space. The dimensions of the detectors employed here are 12.7 mm wide grounded shield and 10.16 mm detector image detection tube length with 4.75 mm OD and 4.11 mm ID. This choice of parameters yields rise times that are typically around 1 μs with a capacitance per tube on the order of 1 pF while allowing a reasonable angular range for the ions to travel through the array.

Our approach to collecting and processing the data is to record unprocessed signals with as wide a bandwidth as reasonable and then to analyze these signals with the computer using digital filters. This approach provides more flexibility than using an analog bandpass filter before the data is recorded. The image charge is detected with preamplifiers based around an Amptek A250. The preamplifiers are located in the vacuum chamber as close to the detector array as possible. The output of each preamplifier is fed to an inverting and noninverting amplifier. The outputs from these amplifiers are passed out of the vacuum chamber and fed directly to the differential input of an analog to digital converter which samples at approximately 2 MHz with 15 bits of resolution.The ADC units output the data over fiber optic connections to a computer for storage and offline processing.

An example of the raw output signal is shown in Figure 2. This signal is the unprocessed output of one charge detection amplifier for a highly charged macroion (2500 e). In this example, it is easy to identify the responses from the 11 detection tubes as the macroion travels through them. The rms noise on the raw unprocessed signal is approximately 490 electrons. We caution the reader not to compare the rms noise we report for the raw signal to the noise reported by others for signals processed by band-pass filters.

The charge scale on the right in Figure 2 is calibrated by putting a test charge onto the detection cylinders and measuring the system response. The test charge is obtained from a voltage pulse using a capacitor (nine 6.8 pF 1% capacitors connected in series).

■ DATA PROCESSING

A number of approaches were considered to process the data. Previously time domain point averaging[10] and FFT (fast Fourier transform)[9,10] methods have been used to analyze repetitive CDMS signals.

To maximize the signal-to-noise ratio in time domain signal averaging, it is necessary to only average over the portion of the time domain signal that contains the signals from the ion. Thus, the use of time domain signal averaging in this application is only appropriate for signals that significantly extend above the noise floor (because it is necessary to locate the signals precisely before averaging them together). The FFT method suffers from poor frequency resolution for signals containing a relatively small number of repeating cycles, like that resulting from the 22 detectors used here. We found that the approach that yielded the highest charge and frequency accuracy was to selectively autocorrelate the data and then correlate the output of this signal to an expected output pattern. This method affords very accurate velocity and charge values. A Fortran program was written to process the data using this approach.

The first step in processing the data is to locate a signal. This is accomplished by stepping an autocorrelation function across the signal. We take $f(t)$ to be the raw signal from the digitizer, $a(t,w)$ to be a rolling average from t to $t + w$, and w to be the total length of the signal (the time the ion spends in the detector array). Note that w is not known, and so, we step through reasonable values of w consistent with the time resolution to get a reconstructed signal given by

$$g(t,w) = c(w) \sum_{k=3}^{20} b(k) \left| \sum_{n=0}^{w} (f(t+n) - a(t,w)) * \left(f\left(t+n+\frac{wk}{22}\right) - a(t,w) \right) \right|^{1/2} \tag{1}$$

If $(n + ((wk)/22)) > w)$, $(n + ((wk)/22))$ in the second term in the summation is replaced with $(n + ((wk)/22) - w)$ so that it wraps around to small values. $c(w)$ in eq 1 is a normalization factor. $b(k)$ is set to +1 for even k and −1 for odd. For the correct value of w, eq 1 preferentially amplifies repetitive in-phase signals to yield a triangular output with a width that is twice the length of the signal. For values of w that are larger or smaller than the correct value, the triangular waveform is truncated to yield a trapezoid.

A key advantage of the function employed here is its response to sharp spikes and steps in the baseline. In other approaches that we tried, we found false positives from spikes and steps to be a significant problem. With the function used, here the spikes and steps are attenuated by around 10^6 and 10^2, respectively.

After the function $g(t,w)$ is generated, it is passed through a low pass filter to remove unwanted high frequency components. For the correct value of w, $g(t,w)$ is expected to be a triangular waveform, and so the best performance should be obtained from a triangular smoothing function. However, we found that smoothing with a triangular function is computationally expensive, and so instead, we employed a filter consisting of four boxcar filters to approximate the triangular shape:

$$G(t,w) = \sum_{m=1}^{4} \sum_{n=-\frac{w+m}{10}}^{\frac{w+m}{10}} g(t,w) \tag{2}$$

This filter is much faster than a full triangular smoothing function, with a performance that is within a few percent of the triangular function.
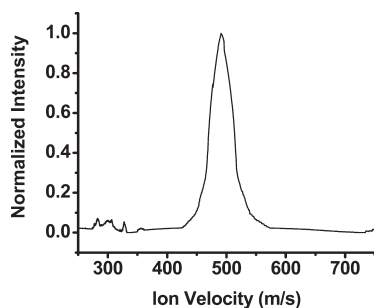
Figure 3. Response of the correlation analysis to an ion traveling through one group of detectors at 491 m/s. The normalized output amplitude of the correlation analysis is plotted against w in terms of the ion velocity.
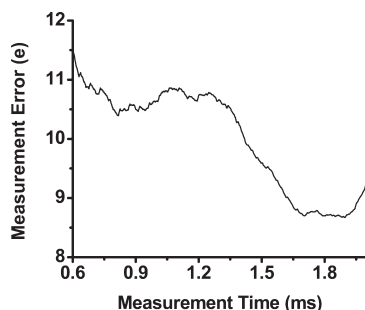

Figure 4. Plot of typical rms error output from the correlation analysis described in the text. The vertical axis is the rms error in units of elementary charge while the horizontal axis shows the parameter w over the relevant times for ions to travel through the detector array.

$g(t,w)$ and the smoothed $G(t,w)$ both yield triangular waveforms with the correct value of w. Away from the correct value of w, both functions are truncated to a trapezoid. The correct value for w is determined by doing calculations with a range of different w values (consistent with the experimental time resolution) and then selecting the value that has the largest amplitude. The amplitude of the triangular waveform provides the charge, and the width is related to the velocity of the ion. Figure 3 illustrates the response of the correlation analysis to an ion traveling through one group of detectors at 491 m/s. The figure shows the normalized output amplitude of the correlation analysis plotted against w in terms of the ion velocity. The peak at 491 m/s indicates the correct velocity. The small features at around 300 m/s are due to overtones.

A typical noise profile for the output of the $G(t,w)$ function is shown in Figure 4. This was generated by analyzing a blank data set (i.e., a data set without an ion signal). The plot shows the rms deviation of the signal as a function of the time w. For white noise, the rms deviation should decrease as $t^{-1/2}$. The broad peak in the noise at around 1.2 ms results from ∼4 kHz interference present in the room from an unknown source. Beyond around 2 ms, $1/f$ noise becomes dominant and the noise ramps up to 20−30 e at ∼4 ms. In the 0.6 to 1.8 ms region of interest, the rms noise is 9−11 e. This limits the accuracy of the charge measurement. The noise can be reduced further by calculating more than just the peak values in the autocorrelation as well as using a full triangular smoothing function. These improvements will be implemented in the future.

■ DATA ANALYSIS

The experimental parameters obtained from the data processing are the initial velocity, the shifted velocity, and the charge.

In addition, we know the voltage change used to shift the velocity. From conservation of energy:

$$\frac{1}{2}mv_{SHIFTED}^2 = \frac{1}{2}mv_{INITIAL}^2 - qV \quad (3)$$

where m is the mass of the ion, q is the charge, $v_{SHIFTED}$ and $v_{INITIAL}$ are the shifted and initial velocities, and the effect of the voltage change V is to decelerate the ions. Deceleration provides better mass resolution than acceleration. For the results reported here, the voltage on the second group of detectors was set to $+1$ V with respect to the first. This value is best for the detection of ions with relatively small m/z values. A larger offset voltage is better for ions with larger m/z values. Equation 3 can be rearranged to yield an expression for the mass:

$$m = \frac{2qV}{v_{INITIAL}^2 - v_{SHIFTED}^2} \quad (4)$$

Inserting the measured values into this equation yields a mass for each ion which can then be binned into a histogram to yield an m spectrum (in contrast to the m/z spectrum usually obtained from mass spectrometry measurements). We use m spectrum instead of mass spectrum because the latter is often used to identify an m/z spectrum.

■ RESULTS

The results for the electrospray of 300 kDa PEG are divided into two parts. First, we show the results for ions with a mass of less than 1 MDa. Then, we show all the data where the velocity is shifted by at least 1%. We do not show data with velocity shifts <1% because the m/z value deduced from the shift becomes less reliable as the shift decreases (see below).

Figure 5 shows mass, m/z ratio, and charge state distributions for ions with a mass of less than 1 MDa. The mass distribution (top panel) shows a broad peak centered around 320 kDa with a full width at half maximum (fwhm) of around 240 kDa. The width of the peak in the mass distribution is mainly due to the heterogeneous nature of the sample (see below). The middle panel in Figure 5 shows the measured m/z distribution. The peak in this distribution is centered at around 2000 Da/e. The bottom panel in Figure 5 shows the charge distribution which extends from 100 to 400 e. In this work, we truncated the charge distribution and did not attempt to analyze results where the charge is less than 100 e. We did this because a nonGaussian noise contribution leads to false positives, but the number of false positives becomes vanishingly small if we truncate the charge in this way.

Figure 6 shows the velocity distributions measured in the two groups of detectors. The initial velocities have a peak centered around 425 ms^{-1}, with a high velocity tail extending to almost 600 ms^{-1}. After deceleration, the peak in the velocities is shifted to around 280 ms^{-1}. The substantial shift in the velocities enhances the accuracy of the m/z values deduced from the velocity shift. However, the uncertainty in the m/z values deduced in this way is around 5%. As we discuss below, this relatively large uncertainty in the m/z values for ions with masses less than 1 MDa results mainly from their relatively low charge. The low charge leads to a low signal-to-noise ratio which makes it difficult to determine the velocities accurately.

We now discuss all the data where the velocity was shifted by at least 1%. These results are shown in Figure 7 which shows the mass, m/z, and charge distributions. The top panel in Figure 7 shows the mass distribution which contains at least three
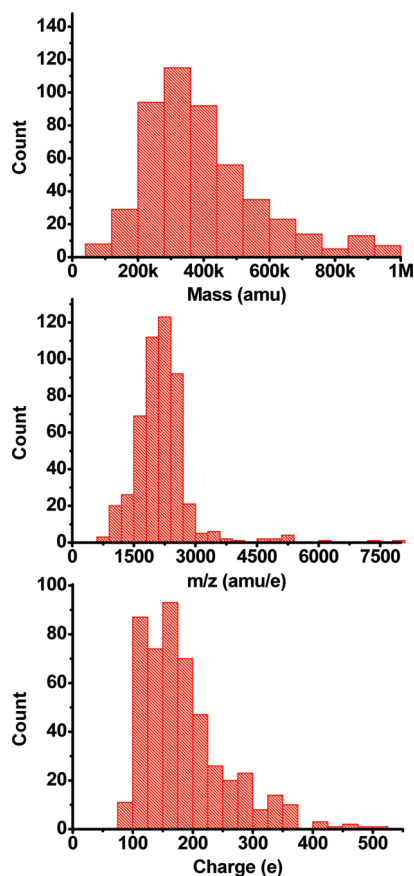
Figure 5. Plots showing results for ions with masses less than 1 MDa. The top panel shows the mass distribution; the middle panel shows the *m/z* distribution, and the bottom panel shows the charge distribution.

components. The peak at lowest mass (close to the origin) consists mainly of the relatively low *m/z* and low charge ions with masses around 300 kDa (which are discussed above). In addition, there are two other peaks at around 100 and 500 MDa. There may be another peak at around 1.25 GDa, but it is too poorly defined to be sure. Masses are observed to beyond 2 GDa. The middle panel in Figure 7 shows the *m/z* distribution for ions with velocity shifts of at least 1%. This distribution shows two components: the lower charge one with a peak near the origin corresponds to the low *m/z* ions that contribute the mass peak at around 300 kDa. The large peak in the *m/z* distribution at around 40 kDa/e is due to the higher mass features in the mass distribution (i.e., the peaks at around 100 and 500 MDa). The bottom panel in Figure 7 shows the charge distribution for ions with velocity shifts of at least 1%. The charge distribution looks similar to the mass distribution because the charge shows a correlation with the mass. Thus, the peak in the charge distribution at around 3000 e is due to ions with masses around 100 MDa, and the broad peak in the charge distribution at around 12 500 e is due to ions with masses of around 500 MDa.

The larger signals obtained for the 100 and 500 MDa ions means that their velocities can be determined much more accurately than for the 300 kDa ions. However, the velocity shifts are smaller, and overall the *m/z* values derived for the larger ions are less reliable than for the smaller ones. The uncertainties in the *m/z* ratios for the heavier ions are around 10−20%. Much more reliable *m/z* values could be obtained for the larger ions using a
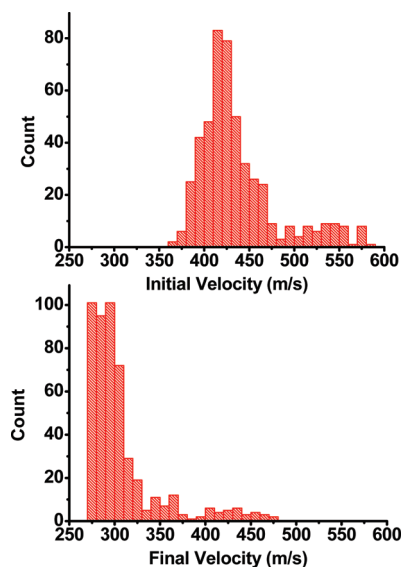

Figure 6. Plots showing velocity distributions for ions with masses less than 1 MDa. The upper panel shows the velocity distribution measured with the first group of detectors. The lower panel shows the velocity distribution measured with the second group of detectors after the ions have been decelerated.
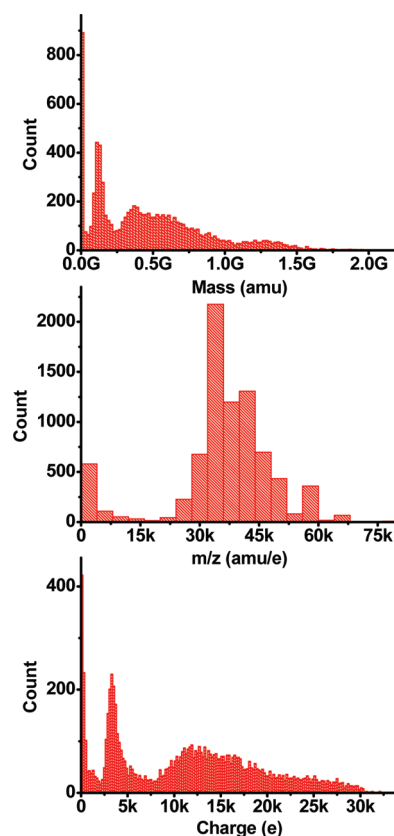

Figure 7. Results for all ions with velocity shifts of at least 1%. The top panel shows the mass distribution; the middle panel shows the *m/z* distribution, and the bottom panel shows the charge distribution.

higher voltage on the second group of detectors (the higher voltage will lead to a larger velocity shift). We did not increase the voltage for the results reported here because our main focus is on the lighter

ions (around 300 kDa), and significantly raising the voltage on the second detector would discriminate against the lighter ions.

There are some ions with velocity shifts that are less than 1%. These ions have m/z ratios that are around 100 kDa/e and masses that extend up to 10 GDa. However, we do not show these results because the uncertainty in the m/z is so large.

■ DISCUSSION

Combined Uncertainty of the Mass Measurements. The uncertainty in the masses obtained from the image charge detector array is a combination of the uncertainties in the m/z ratio and the charge. The relative uncertainty in the m/z values is given by the following equation:

$$\frac{\sigma_{m/z}}{m/z} = \frac{1}{v_{INITIAL}^2 - v_{SHIFTED}^2}\sqrt{(2v_{INITIAL}\sigma_{VINITIAL})^2 + (2v_{SHIFTED}\sigma_{VSHIFTED})^2}$$

(5)

where $\sigma_{VINITIAL}$ and $\sigma_{VSHIFTED}$ are the uncertainties in the initial and shifted velocities, respectively. The uncertainty in the m/z values increases when the difference between the initial and shifted velocities decreases and when the uncertainties in the initial and shifted velocities increase. The uncertainty in the velocities depends on the charge of the ion. When the charge on the ion is small, the unfavorable signal-to-noise ratio means that it is difficult to determine the velocity accurately. The uncertainty in the velocities from this source can be estimated from Figure 3 which shows the normalized response of the digital filter used to analyze the signals from the image charge detector array plotted against ion velocity. If the signal-to-noise ratio approaches infinity, then the velocity is precisely defined at the maximum in the plot, but if the signal-to-noise ratio is 2, then the uncertainty in the velocity error can be estimated from half of the fwhm of the peak, which is 4.5%. For the ions examined here, the uncertainty in the charge is 10% or less. The corresponding uncertainty in the velocity can be estimated from half the width of the response peak in Figure 3 at a normalized intensity of 0.9 (or more). Thus, the uncertainty in the velocity determinations from this source is, at worst, 1.4%.

Most of the ions with m/z values centered around 2000 Da/e have charges of 100–200 e, and so, the maximum uncertainty in the charge is approximately 10%. This yields a maximum mass to charge (m/z) uncertainty of approximately 5% and a maximum combined mass uncertainty of 11%. For the ions with m/z values centered about 40 kDa/e, the charge is around 10 000 e, and so, the relative uncertainty in the charge is much smaller (around 0.1%). Thus, the uncertainty in the velocities from the noise on the charge is also much smaller than for the ions with m/z around 2000 Da/e. However, the velocity shift for the 40 kDa/e ions is much less than for the 2000 Da/e ions since the offset voltage on the second set of detectors to shift the velocity was optimized for the lower mass ion measurements. Therefore, the uncertainty in the m/z values for these ions is approximately 15% and quickly becomes larger as the velocity shift decreases further. For the highly charged ions, the combined uncertainty in the mass is dominated by the small change in velocity and it is, therefore, 15%. With a velocity shift voltage of 20 V (instead of the 1 V used in these measurements), the combined uncertainty in the mass would drop below 1%.

m Spectrum Measured for 300 kDa PEG. The m spectrum measured for 300 kDa PEG shows a broad peak centered around 300 kDa and then peaks at around 100 and 500 MDa. All of these peaks are reproducible and were observed in multiple runs. The 300 kDa peak is broad; however, this is not due to uncertainty in the mass measurements because (as outlined above) the maximum uncertainty expected in this mass regime is 11%. Most of the width of the measured distribution is intrinsic to the PEG sample. The distributor (Polysciences) quotes a distribution that extends from 0.5 to 1.5 times the average mass. Our measured distribution starts at around 150 kDa, peaks at around 320 kDa, and tails off at around 600 kDa. The slight excess of high mass ions could (1) be intrinsic to the sample, (2) result from incomplete desolvation, or (3) result from the presence of a small amount of dimer.

What is the origin of the peaks in the m spectrum at 100 and 500 MDa? They could be residual water droplets, in which case they would have diameters around 70 and 120 nm, respectively. The problem with this explanation is that droplets of this size should evaporate away very quickly, and it is not clear why these particular sizes should persist. Furthermore, the 100 and 500 MDa peaks were not observed when we electrosprayed other solutions. For example, with a highly diluted PEG solution (around 1 nM), we hardly observed any ions. We also did not observe the 100 and 500 MDa peaks when we electrosprayed a BSA (bovine serum albumin) solution. In this case, the largest ions observed were less than 10 MDa.

Another plausible explanation for the high mass peaks is that they result from aggregates of PEG (around 330 PEG molecules for the 100 MDa peak and around 1670 PEG molecules for the 500 MDa peak). It is possible that the aggregates are present in solution. Alternatively, the aggregates could be the residue from large electrospray droplets. Assuming that the ions are generated by the charge residue model,[13,14] then the electrospray droplets from which the aggregates originate must be at least 1.0 μm diameter for the 100 MDa peak and at least 1.7 μm diameter for the 500 MDa peak (droplets of 1.0 and 1.7 μm diameter contain 330 and 1670 PEG molecules at the concentration employed here). These droplets are around 2 times and 3.4 times larger than expected from the scaling laws for the electrospray conditions (flow rate and solution conductivity) employed here.[15,16] Thus, while it seems likely that the 100 and 500 MDa peaks result from PEG aggregates, it is not clear whether the aggregates are the residues of large electrospray droplets or result from incomplete dispersion of the PEG in solution.

■ CONCLUDING REMARKS

The main technical advances described here are (1) the use of a charge detector array with two groups of detectors biased at different voltages to determine the m/z ratio without prior knowledge of the ion energy and (2) the use of a correlation method to analyze the output from the image charge detector array.

These developments allow an accurate determination of the charge for macroions with charges 2.5 times lower than the previously reported for a direct charge detection scheme. The ability to measure small charges accurately allows us to determine the masses of single ions around an order of magnitude smaller than previously reported for charge detection mass spectrometry.[7−11] The uncertainty in the mass measurements for the 300 kDa PEG ions is still relatively large (maximum of 11%).

■ AUTHOR INFORMATION

Corresponding Author
*E-mail: mfj@indiana.edu.

F

dx.doi.org/10.1021/ac102633p |*Anal. Chem.* XXXX, XXX, 000–000

■ ACKNOWLEDGMENT

■ REFERENCES

(1) Ekinci, K. L.; Huang, X. M. H.; Roukes, M. L. *App. Phys. Lett.* **2004,** *84*, 4469–4471.

(2) Yang, Y. T.; Callegari, C.; Feng, X. L.; Ekinci, K. L.; Roukes, M. L. *Nano Lett.* **2006,** *6*, 583–586.

(3) Shelton, H.; Hendricks, C. D.; Wuerker *J. App. Phys.* **1960,** *31*, 1243–1246.

(4) Keaton, P. W.; Idzorek, G. C.; Rowton, L. J.; Seagrave, J. D.; Stradling, G. L.; Bergeson, S. D.; Collopy, M. T.; Curling, H. L.; McColl, D. B.; Smith, J. D. *Int. J. Impact Eng.* **1990,** *10*, 295–308.

(5) Stradling, G. L.; Idzorek, G. C.; Shafer, B. P.; Curling, H. L.; Collopy, M. T.; Blossom, A. A. H.; Fuerstenau, S. *Int. J. Impact Eng.* **1993,** *14*, 719–727.

(6) Hendricks, C. D. *J. Colloid Sci.* **1962,** *17*, 249–259.

(7) Fuerstenau, S. D.; Benner, W. H. *Rapid Commun. Mass Spectrom.* **1995,** *9*, 1528–1538.

(8) Schultz, J. C.; Hack, C. A.; Benner, W. H. *J. Am. Soc. Mass Spectrom.* **1998,** *9*, 305–313.

(9) Fuerstenau, S. D.; Benner, W. H.; Thomas, J. J.; Brugidou, C.; Bothner, B.; Siuzdak, G. *Angew. Chem., Int. Ed.* **2001,** *40*, 541–544.

(10) Benner, W. H. *Anal. Chem.* **1997,** *69*, 4162–4168.

(11) Gamero-Castaño, M. *Rev. Sci. Instrum.* **2007,** *78*, 043301.

(12) Scientific Instrument Services, Inc., Ringoes, NJ, www.simion.com.

(13) Dole, M.; Mack, L. L.; Hines, R. L.; Mobley, R. C.; Ferguson, L. D.; Alice, M. B. *J. Chem. Phys.* **1968,** *49*, 2240–2249.

(14) Mack, L. L.; Kralik, P.; Rheude, A.; Dole, M. *J. Chem. Phys.* **1970,** *52*, 4977–4986.

(15) Gañán-Calvo, A. M.; Dávila, J.; Barrero, A. *J. Aerosol Sci.* **1997,** *28*, 249–275.

(16) Lenggoro, I. W.; Okuyama, K.; Fernández de la Mora, J.; Tohge, N. *J. Aerosol Sci.* **2000,** *31*, 121–136.